Renewable Energy 37 (2012) 82–88

Contents lists available at ScienceDirect

Renewable Energy

journal homepage: www.elsevier.com/locate/renene

Photovoltaic applications for off-grid electrification using novel multi-level inverter technology with energy storage

Kapila Bandara [a], Tracy Sweet [b,*], Janaka Ekanayake [b]

[a] Ceylon Electricity Board, Sri Lanka
[b] The Institute of Energy, Cardiff School of Engineering, Cardiff University, CF24 3AA, Wales, UK

ARTICLE INFO

Article history:
Received 5 January 2011
Accepted 23 May 2011
Available online 30 June 2011

Keywords:
Renewable energy
Inverter
Photovoltaic
Off-grid
Battery
Efficiency

ABSTRACT

In areas where grid connection is difficult and costly, the use of renewable energy is both economically and environmentally advantageous. Due to typically low system efficiency (~10%) and intermittency of photovoltaic (PV) electricity generation, a new design of multi-level H-bridge inverter technology is considered. This multi-level technology increases DC to AC conversion efficiency and the design includes battery energy storage to enable 24/7 operation. The proposed multi-level inverter is compared and contrasted with other existing designs. The proposed cascaded inverter provides lower switching losses, simple switching techniques, modularity, and simpler charge-balancing approaches than conventional technology. A switching technique was designed for the proposed multi-level inverter to ensure balancing of state of charge of each battery. The effectiveness of the switching was demonstrated via simulations. The simulations also show that the total harmonic voltage distortion of the proposed inverter is less than 6% without any filtering requirements.

1. Introduction

Photovoltaic (PV) technologies provide clean, secure and reliable renewable energy sources with extremely low running costs, no moving parts, minimal maintenance requirements, zero fuel cost and long lifetimes (20+ years). These advantages make the application of PV in off-grid installations both technologically feasible and economically viable. PV has been proven to meet some of society's future energy requirements in a sustainable, non-polluting manner. In India, 450 000 off-grid solar PV systems (typically 35–100 Wp capacity) were deployed (Ministry of New and Renewable Energy, 2009) [1]. The majority of the populations in developing countries, such as Nepal (61%), still have no access to electricity. Governments have now prioritized rural electrification and solar PV is one of the most commonly adopted off-grid technologies [2].

One of the classic examples of off-grid PV applications is a 1 kW PV array at the Van Geet Off-Grid home [3] in Colorado. In this example, the cost of extending the electrical power grid 1.5 miles to reach the building was estimated as US$ 100 000; therefore utilizing an amorphous Silicon PV array, with a maximum power point tracking (MPPT) controller, 42.7 kWh battery bank and 4 kW inverter, in combination with energy efficient building design, proved highly successful in both economic and environmental terms.

In 2010, where global shipment of PV exceeded 16 GWp, crystalline Silicon materials accounted for 87% of the market [4]. Even though world-class polycrystalline silicon cell efficiencies as high as 20.3% have been reported [5], a typical commercially available polycrystalline silicon module with published efficiency of 13.4% [6] was selected as a basis for this study. Electricity generation from a PV array is intermittent due to the requirement for photons provided by sunlight. PV arrays produce no electricity at night and generate less than maximum (peak power) during cloudy climatic conditions or if partial shading occurs. These factors necessitate battery energy storage for continuous electricity supply in off-grid applications.

The generated DC from a PV array is first converted into AC by an inverter which has published practical efficiencies ranging from 85.8% [7] to 92.4% [8] (peak efficiency). However when a standard inverter is used with a poly-silicon PV array the overall system efficiency becomes about 10%. With such low conversion efficiency, the losses associated with an inverter should be minimised.

In this paper, a 13-level cascaded multi-level inverter with low switching frequency is introduced for off-grid applications. As the voltage produced by a solar array is low, a step up transformer or

* Corresponding author. Tel.: +44 0 29 2087 0673.
E-mail address: sweett@cardiff.ac.uk (T. Sweet).

0960-1481/$ – see front matter © 2011 Elsevier Ltd. All rights reserved.
doi:10.1016/j.renene.2011.05.036

a DC–DC boost converter is commonly used to obtain 230 V at the output. Commonly pulse width modulation (PWM) inverters are employed for DC to AC conversion. However, because of high dv/dt stress on switching devices, high losses, electromagnetic interference (EMI) problem and higher total harmonic distortion (THD) levels, multi-level inverter are now being considered [9,10].

This paper is organized as follows: in the next section the photovoltaic system is outlined together with the new cascade inverter design and switching pulse generator. Section 2.3 presents the battery model and Section 2.4 presents the PV model. A comparison of inverter topologies is given in Section 3 and Section 4 presents simulation results and discussions. Section 5 concludes our study.

2. Photovoltaic system

The complete off-grid PV system was designed with six PV arrays, each having 5 parallel connected modules; each module containing 90 cells, MPP 55–60 V with 135 W output.

2.1. 13-Levels cascaded inverter

Fig. 1 shows the circuit diagram of the 13-level cascaded inverter. In this inverter, there are six H-Bridges which are connected in series and operating at fundamental frequency. Compare to the other multi-level topologies such as diode clamp, flying capacitor, cascaded H-Bridge PWM and cascaded transformer PWM, this inverter has many advantages [9–11]. These include low switching losses, simple switching techniques and minimum components. Further, this configuration does not need advanced charge-balancing techniques or complex switching techniques for minimizing losses as in diode clamp and flying capacitor inverters.

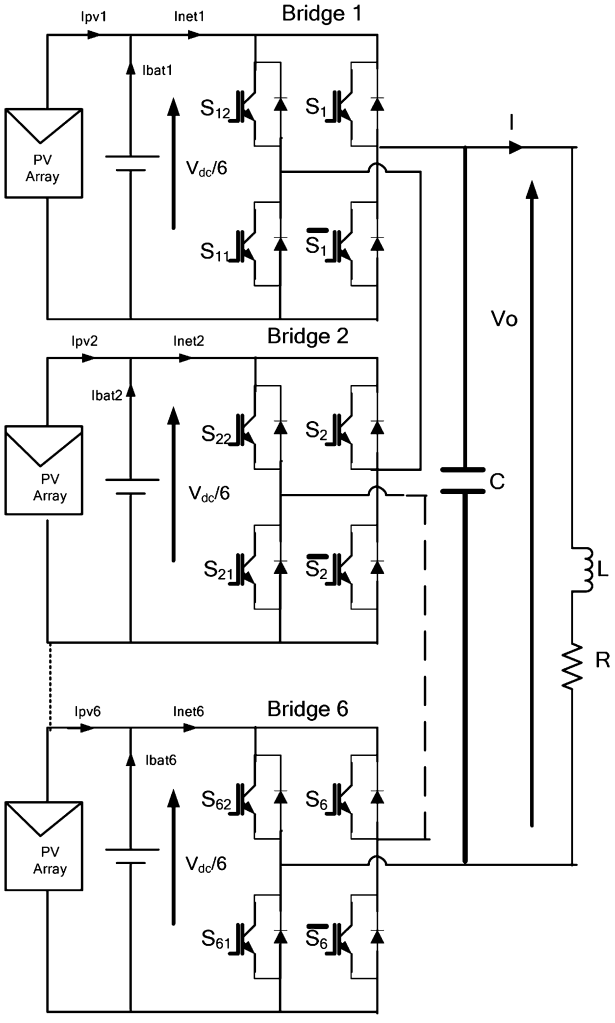

Fig. 1. 13 Levels H-Bridge converter 2.1.2 Switching topology.

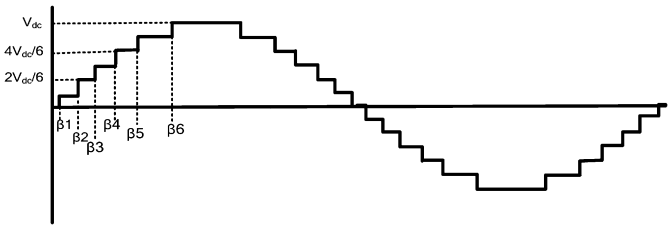

Fig. 2. 13-level H-Bridge output voltage.

As shown in Fig. 1, six isolated photovoltaic systems parallel with a battery pack have been connected to each H-Bridge. The voltage levels of the battery energy storage and PV system are designed such that the fundamental component of the inverter output voltage is equal to 230 V. A 100 μF capacitor is connected across the inverter output which works as a power factor correction capacitor as well as a harmonic filter.

In order to obtain 13 voltage levels (shown in Fig. 2) with series connected H-Bridges as shown in Fig. 1, the switching patterns given in Tables 1 and 2 were applied. Each H-Bridge is a 3-level inverter and is capable of generating output voltage of $+V_{dc}/6$, 0, $-V_{dc}/6$ (where V_{dc} is the peak of the multi-level voltage output shown in Fig. 2) depending on the switching state. To obtain positive output voltages, switches S_1, S_2 S_3, S_4, S_5 and S_6 should be on and $\overline{s_1}$, $\overline{s_2}$, $\overline{s_3}$, $\overline{s_4}$, $\overline{s_5}$ and $\overline{s_6}$ off. Alternatively, to obtain negative output voltages, $\overline{s_1}$, $\overline{s_2}$, $\overline{s_3}$, $\overline{s_4}$, $\overline{s_5}$ and $\overline{s_6}$ are on while S_1, S_2, S_3, S_4, S_5 and S_6 are off. In this inverter, to obtain different voltage steps six bridges were switched at different switching delays, β1, β2, …, β6, as shown in Fig. 2. To optimize the fundamental voltage component with minimum total harmonic distortion, β1, β2, …, β6 are chosen as 5^0, 15^0, 25^0, 36^0, 49^0 and 67^0 respectively.

2.2. Switching pulse generator

A switching pulse generator for each H-Bridge consists of a signal generator and a signal comparator. The signal generator produces unity gain sinusoidal modulating signal with period T and a staircase like carrier signal with period 6T (as shown in Fig. 3). At the signal comparator the modulating signal and the carrier signal are compared to produce switching signals. Fig. 3 illustrates how a switching signal is generated for switch 1 of H-Bridge 1 for generating positive voltages. As shown in Fig. 3 when the sinusoidal

Table 1
Switching state for the 13-level cascaded H-Bridge for producing positive voltages.

Inverter output voltage (V)	S_1 to S_6	$\overline{s_1}$ to $\overline{s_6}$	S_{11}	S_{21}	S_{31}	S_{41}	S_{51}	S_{61}	S_{12}, S_{22}, S_{32}, S_{42}, S_{52}, S_{62}
0	0	0	0	0	0	0	0	0	0
$V_{dc}/6$	1	0	1	0	0	0	0	0	0
$2V_{dc}/6$	1	0	1	1	0	0	0	0	0
$3V_{dc}/6$	1	0	1	1	1	0	0	0	0
$4V_{dc}/6$	1	0	1	1	1	1	0	0	0
$5V_{dc}/6$	1	0	1	1	1	1	1	0	0
$6V_{dc}/6$	1	0	1	1	1	1	1	1	0

Table 2
Switching State for the 13-level cascaded H-Bridge for producing negative voltages.

Inverter output voltage (V)	S_1 to S_6	$\overline{S_1}$ to $\overline{S_6}$	S_{12}	S_{21}	S_{31}	S_{41}	S_{51}	S_{61}	S_{11}, S_{21}, S_{31}, S_{41}, S_{51}, S_{61}
$-V_{dc}/6$	0	1	1	0	0	0	0	0	0
$-2V_{dc}/6$	0	1	1	1	0	0	0	0	0
$-3V_{dc}/6$	0	1	1	1	1	0	0	0	0
$-4V_{dc}/6$	0	1	1	1	1	1	0	0	0
$-5V_{dc}/6$	0	1	1	1	1	1	1	0	0
$-6V_{dc}/6$	0	1	1	1	1	1	1	1	0

modulating signal is greater than the carrier signal, the signal generator gives an output of 1. Otherwise it gives an output of 0. In the case of generating the switching signal to S_2 (H-Bridge 2), the staircase like carrier signal in Fig. 3 is shifted right by time T s, such that when the carrier signal of Bridge 1 is Sin(β1), the carrier signal of Bridge 2 is Sin(β2).

As discussed above, the switching pulse generator switches on and off the relevant bridge to produce $+V_{dc}/6$, 0 or $-V_{dc}/6$ voltages at its terminal at corresponding delay angles (β1, β2, …, β6). If Bridges 1 to 6 are always switched on at delay angles β1, β2, …, β6 respectively, battery energy storage connected to Bridge 1 delivers maximum energy (as it conducts from β1 to π- β1) while Bridge 6 delivers the lowest amount of energy (it conducts from β6 to π-β6). To avoid this, the delay angle of each bridge is rotated in each cycle such that if Bridges 1 to 6 are switched on with delay angle β1, β2, …, β6 during the first voltage cycle, during the next voltage cycle they are switched on with delay angles β2, β3, …, β1. In this way after 6 cycles, the amount of energy drain from each battery storage becomes equivalent. The switching pulse generator achieves this by comparing the modulating signal with a staircase carrier signal of period of 6T with a six distinct voltage levels at Sin(β1), Sin(β2) Sin(β3), Sin(β4), Sin(β5) and Sin(β6) as shown in Fig. 3. The width of each step of carrier signal is equal to time T.

2.3. Battery model

For this study 1 Ah Lithium Ion battery pack was used as the energy storage system. The dynamic model of a 1 Ah lithium Ion battery has been derived assuming that the internal resistance of the battery does not change. The capacity of the battery does not depend on current amplitude and the battery has no temperature

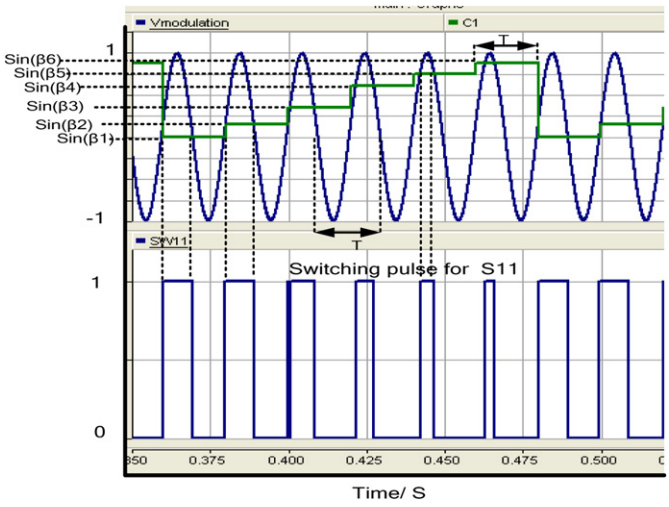

Fig. 3. Generation of switching signal for switch S_1 of the H-Bridge 1 of the inverter.

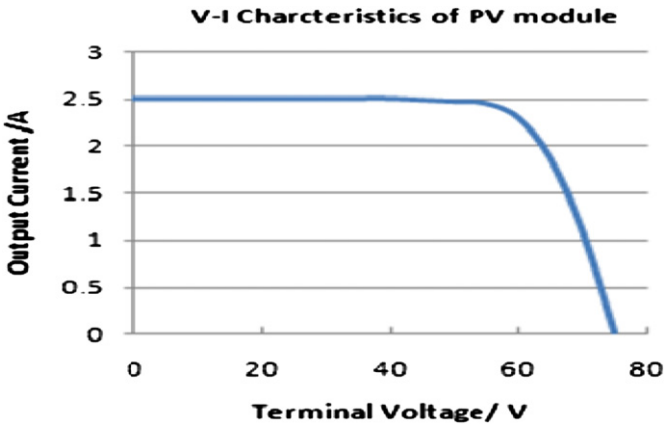

Fig. 4. V–I characteristics of PV module.

effect, memory effect and self discharge [12]. In this study the battery model described in reference [12] was used where the State of Charge (SOC) is the only state variable and net discharge current is the input variable. This model represents the manufacture's curve for three types of industrial batteries: Li-Ion (Lithium ion), NiCd (Nickel Cadmium), and NiMH (Nickel-metal hydride). For the model, open circuit battery voltage based on the actual SOC of the battery is described by following equations:

$$E_{\text{batt}} = E_0 - K\cdot\frac{1-\text{SOC}}{\text{SOC}}\cdot Q + A\cdot e^{-B(1-\text{SOC})\cdot Q} \quad (1)$$

$$V_{\text{batt}} = E_{\text{batt}} - R_{\text{batt}}\cdot I_{\text{batt}}: \quad (2)$$

Where:

E_{batt}: internal voltage (V), E_o: battery voltage constant (V), K: polarisation voltage (V), SOC: state of charge (%), Q: battery capacity (Ah), A: exponential zone amplitude (V), B: exponential zone time constant inverse Ah^{-1}, V_{batt}: terminal voltage (V), I_{batt}: battery current (A), R_{battt}: internal resistance (Ω). The parameters A,B,K,E_o are determined from the manufacture's discharge curve of battery.

2.4. Photovoltaic model

A PV model given in PSCAD/EMTDC was used for the simulation study. This model composed of an ideal current source, a diode connected in parallel and a series resistor. The output current of this model depends on solar irradiance, cell temperature and terminal output. For the model output current is given by:

$$I_A = N_p I_{\text{SC}} - N_p I_o\left(\exp\left[\frac{V_A + I_A R_S}{nN_s V_T}\right] - 1\right) \quad (3)$$

Where:

I_A is output current (A), I_{SC} is short circuit current (A) which depends on solar radiation and cell temperature, N_S is the number of modules in series, N_p is the number of modules in parallel, I_o is diode saturation current (A), V is terminal voltage (V), n is ideal constant of diode, and V_T is thermal potential of module (V).

For the simulation, a PV module which has 90 cells in series, with an open circuit voltage of 75 V and a short circuit current of 2.5 A was used. Fig. 4 shows the V–I characteristic of the PV module. According to the graph, voltage at the maximum power point is between 55 and 60.

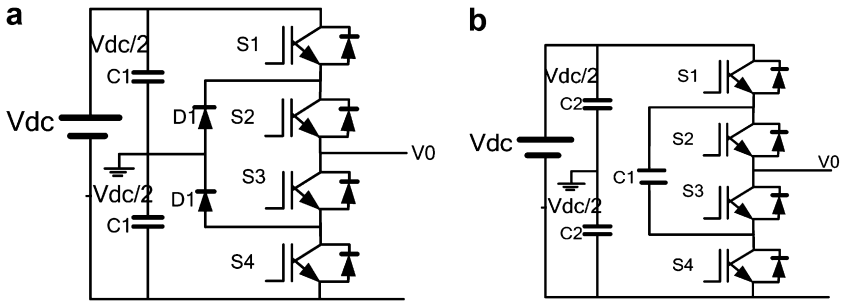

Fig. 5. (a): 3-level diodes clamp inverter. (b): 3-level capacitor clamp inverter.

Table 3
A component level comparison between the proposed 13-level inverter and other multi-level inverters.

Type	Switch	Clamping diode	Balancing capacitor	DC-bus	Transformer
Diode clamp [13]	24	132	NA	12	NA
Flying capacitor [13]	24	NA	66	12	NA
PWM based cascaded H-bridge [9]	24	NA	NA	6	NA
PWM based cascaded transformer [9]	16	NA	NA	1	Cascaded type 4 Level
Proposed 13-level inverter	24	NA	NA	6	NA

3. Comparison of different multi-level inverter topologies

3.1. Component level comparison

Table 3 illustrates the component level comparison between the proposed 13-level inverter and other multi-level inverters reported in the literature [9,13,14]. The configurations selected for this comparison include diode clamp, flying capacitor, PWM based cascaded H-Bridge and PWM based cascaded transformer type multi-level converters. Fig. 5(a) and (b) shows the configuration of 3-level diode clamp and flying capacitor inverters [13]. For the 13-level inverter used for comparison in this study there are 24 series connected insulated gate bipolar transistors (IGBTs). The PWM based cascaded H-Bridge converter has the circuit topology the same as that shown in Fig. 1 but switches in each H-Bridge are switched using a PWM switching pattern [9,14,15]. The PWM based cascaded transformer type multi-level converter is a special design which needs a special transformer with 4 levels [9].

The PWM based cascaded transformer type multi-level converter has the lowest number of switches and independent DC sources, but it needs a special transformer. Even though it has the lowest number of switches, the current flowing through these switches is greater than that of the proposed inverter when both are delivering the same amount of power. Compared with the diode clamp or flying capacitor type inverters, the proposed inverter has a lower number of components because it does not need clamping diodes or balancing capacitors. Further, the proposed inverter is ideal for modularized circuit layouts and packaging [11].

Table 4
A comparison of Switching and transformer losses of a 10 kW inverter.

	Proposed	PWM H-Bridge	Diode clamp	Cascaded transformer
Switching Loss/W	12	450	675	300
Transformer loss/W	NA	NA	NA	275
Cost of cooling device	Low	High	High	High
Size of module	Small	Large	Large	Very large
Switching loss	Low	High	High	High & transformer

3.2. Switching and transformer loss comparison

Real controllable switching devices such as Insulated Gate Bipolar Transistor (IGBT) and Metal-Oxide Semiconductor Field-Effect Transistor (MOSFET) typically have a switch on and off delay of a few nanoseconds. These delays cause a power loss when turning the device on and turning it off. Switching losses in the inverter are proportional to the switching frequency, load current and modulating index [16]. The switching frequency of the proposed inverter is 50 Hz and switching current is approximately 40 A when it is delivering a constant power of 10 kW at unity power factor. If it is assumed that the switches are FGH40N60SFD, 600 V, 40 A Field Stop IGBT, then switching loss of a switch is approximately 0.99 W under the above operating conditions [17]. In the proposed inverter twelve switches are on and off at zero current when it is operating at unity power factor. Within a PWM based multi-level inverter, the switching loss of a switch under same condition is approximately 19.8 W when the switching frequency is 1 kHz. As given in Table 4, the proposed inverter has the maximum efficiency under unity power factor because of low switching frequency and a transformer is not required.

The transformer has its own losses such as winding resistance, hysteresis, and eddy current, stray and mechanical losses. A PWM inverter needs approximately 12 kVA transformer to connect the photovoltaic system to the grid. The efficiency of the 12 kVA transformer is 98% under rated condition, supplying pure sinusoidal current [18,19]. Eddy current loss under rated condition is

Table 5
Circuit parameters of simulated 10 kW 230 V off-grid PV system.

Parameter	Symbol	Value/number with units
Nominal rms Voltage	Vs	230 V
Power Rating	P	10 kW
Number of cascaded inverters	n	6
Coupling inductor	L	0.005 H
Power factor correction capacitor	C	100 μF
Battery pack voltage connected to each H-Bridge	V_{dc}	$230 \times \frac{\sqrt{2}}{6} = 54.5$ V
Li-Ion Batteries in each battery pack		3.9 V, 1 Ah 14 in series and 5 in parallel
Photovoltaic array connected to each H-Bridge		5 in parallel
Short circuit current of a PV cell	I_{SC}	2.5 A
Number of series cells per module	N_S	90
Terminal voltage at maximum power point of module(Simulation)		55–60 V

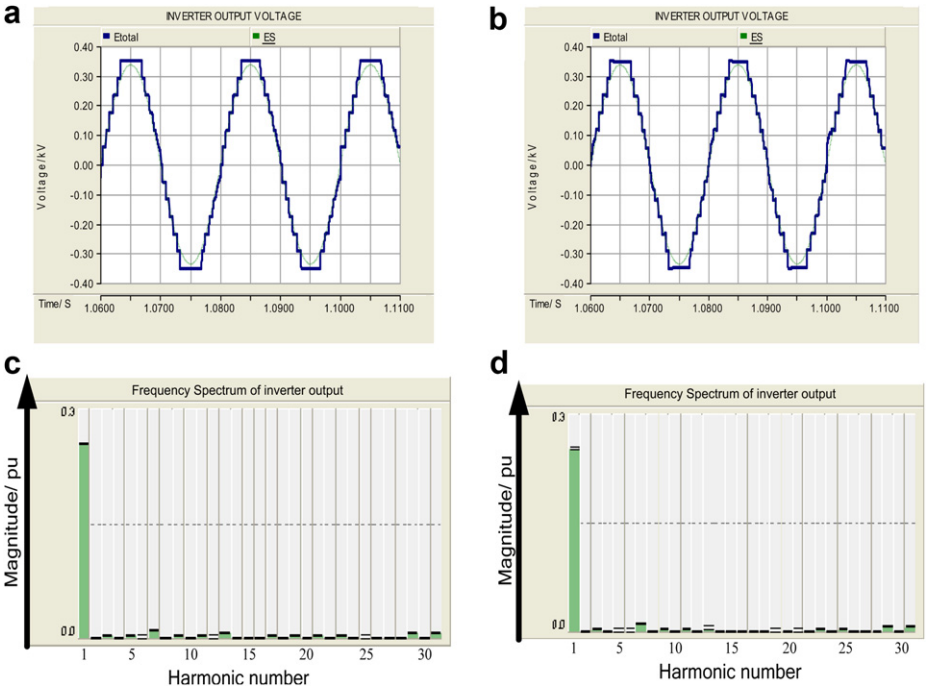

Fig. 6. Steady state inverter output voltage and frequency spectrum. (a): Output voltage at unity power factor. (b): Output voltage at 0.95 lagging pf. (c): Frequency spectrum (THD = 4.9) at unity power factor. (d): Frequency spectrum (THD = 5.6) at 0.95 power factor.

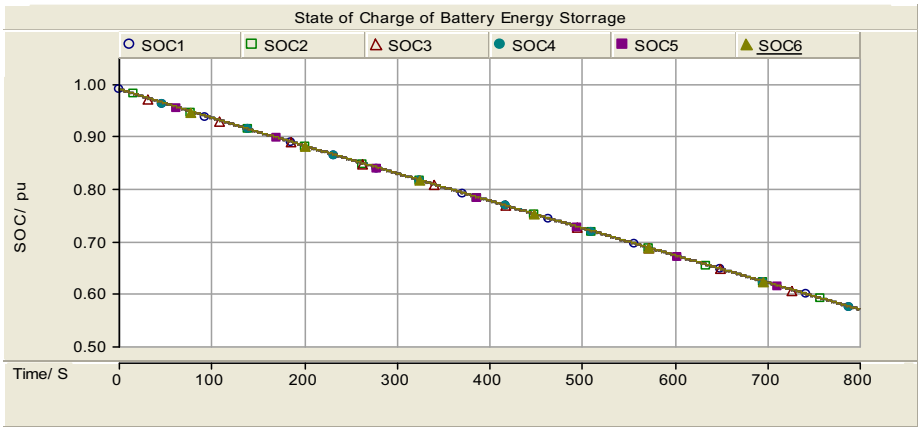

Fig. 7. SOC of all the batteries under same irradiance (600 W/m^2)

assumed as 15% of total loss [19] and eddy current loss factor at 1 kHz switching frequency is 2.53 [20]. Approximate total transformer loss in PWM based cascaded transformer inverter operating at 1 kHz switching frequency is 275 W when it is delivering 10 kW of power.

4. Simulations and result

4.1. System description

A 10 kW, 230 V off-grid PV system based on the proposed inverter shown in Fig. 1 was used for this study. The system parameters are given in Table 5 (some parameters are marked in Fig. 1). This system was simulated in PSCAD/EMTDC software to observe the performance of the proposed inverter and its control.

4.2. Inverter output voltage under steady state operation

The output voltage waveform and its frequency spectrum were obtained from simulations when the system was operating at unity

Table 6
Irradiation patterns.

Time/S	Irradiance on PV module 1–3 W/m^2	Irradiance on PV module 4–6 W/m^2
01–100	350	800
100–200	445	575
200–300	690	655
300–400	800	750
400–500	750	800
500–600	655	690
600–700	575	445
700–800	800	350

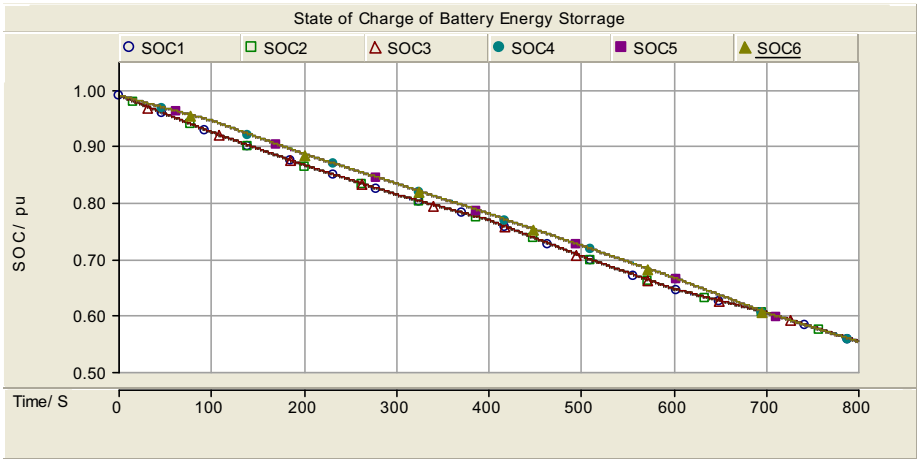

Fig. 8. SOC of all battery energy storage system under different irradiance.

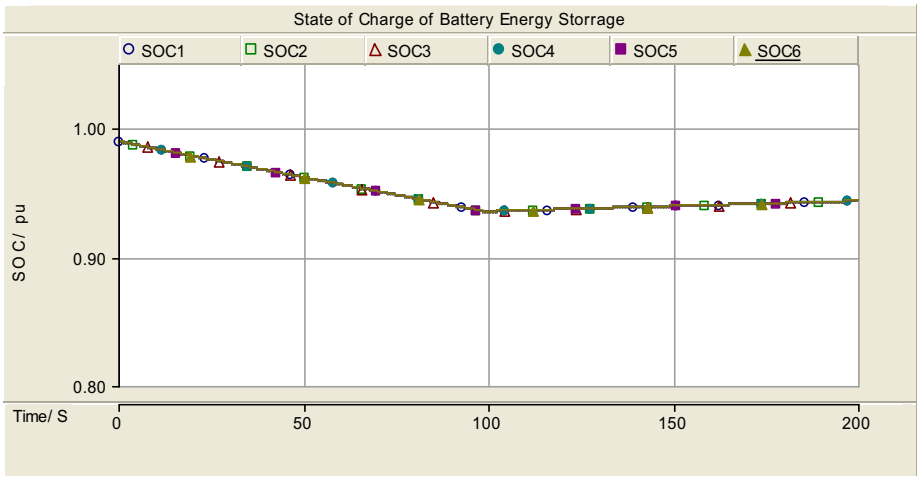

Fig. 9. The SOC of the battery energy storage at 10 kW and 2 kW.

and 0.95 power factor (typical lagging power factor expected in an off-grid installation). In both cases the output load was 10 kW. As shown in Fig. 6, in both cases the output voltage of the inverter is very close to a pure sinusoidal waveform and the Total Harmonic Distortion of the inverter output voltage when operating at unity and 0.95 power factor were 4.9% and 5.6% respectively.

4.3. State of charge (SOC) balancing under constant irradiance

To investigate the performance of SOC balancing techniques, the system was simulated for 800 s giving constant irradiance (600 W/m^2) to all PV modules. It was assumed that the power output was 10 kW, with a cell temperature of 25 °C. Fig. 7 shows the SOC of all of the batteries. It can be clearly seen that the SOC at any given time in all the batteries are the same thus demonstrating the effectiveness of the proposed SOC balancing control.

4.4. SOC balancing under different irradiance

To observe the performance of SOC balancing techniques under different irradiance conditions, the PV system was simulated under different irradiance patterns on PV modules 1–6. Table 6 gives the irradiance on each PV module and Fig. 8 shows the simulation result. Even though there is a slight deviation of SOC levels of each battery, they are almost identical.

4.5. System behaviour under low load

Finally, to see the system behaviour under low load condition, at $t = 100$ s, the output of the PV system was reduced from 10 kW to 2 kW and the SOC of all of the batteries was observed. As shown in Fig. 9, from 0 to 100 s both PV modules and batteries supply power. However, when the output load is low the PV modules charge the batteries to increase the SOC.

5. Conclusions

This paper presents an off-grid PV system which employs a 13-level cascaded inverter without a transformer. Different multi-level power inverters were compared and contrasted with the proposed inverter for a PV system with battery energy storage. The proposed cascaded inverter provides lower switching losses, a simple switching technique, modularity, and simpler charge-balancing approaches.

A switching technique which could balance the SOC of all of the battery packs was proposed and its effectiveness was demonstrated via simulations. From simulations it was found that the proposed controller not only balances the SOC level of each battery pack but

also reduces the THD at the output to be less than 6% without any harmonic filtering.

Acknowledgements

The first author would like to thank the Commonwealth Scholarship Commission, British Council UK and the Association of Commonwealth Universities for their support and providing funding for his Professional Fellowship. Authors would also like to acknowledge the support of the Low Carbon Research Institute (LCRI), the Higher Education Funding Council for Wales (HEFCW) and the UK Energy Research Council (UKERC).

References

[1] Chaurey A, Kandpal TC. A techno-economic comparison of rural electrification based on solar home systems and PV microgrids. Energy Policy 2010;38: 3118–29.
[2] Mainali B, Silveira S. Financing off-grid rural electrification: country case Nepal. Energy April 2011;36(4):2194–201.
[3] Dennis Barley C, Torcellini P, Van Geet O. Design and performance of the Van Geet off grid home. Journal of Solar Energy Engineering, Transactions-of-the-ASME 2004;126:738–43. May 2004.
[4] Mints P. PV sector market forecast. Thin-film in the era of cheap crystalline PV. Renewable Energy World January–February 2011;14(1).
[5] Vazmerski L, National renewable energy Laboratory, National Centre for Photovoltaics. World-class efficiencies timeline. Accessed online, 20th November 2010, http://www.nrel.gov/docs; 2010.
[6] Product data sheet for polycrystalline commercial module ND-220E1F document, online [Accessed online: 18th November 2010, http://www.sharpmanufacturing.co.uk/cps/rde/xchg/sukm/hs.xsl/-/html/product_details.htm?product=ND220E1F&cat=46005.
[7] Mondol D, Yohanis YG, Norton B. The effect of low insolation conditions and inverter oversizing on the long-term performance of a grid-connected photovoltaic system. Progress in Photovoltaics: Research and Applications 2007;15(4):353–68.
[8] Mazumder K, Burra RK, Acharya K. A ripple-mitigating and energy-efficient fuel cell power-conditioning system. IEEE Transactions on Power Electronics 2007;22(4):1437–52. 38.
[9] Kang Feel-Soon, Park Sung-Jun, Eog Cho Su, Kim Cheul-U, Ise Toshifumi. Multilevel PWM inverters suitable for the use of stand-alone photovoltaic power systems. IEEE Transactions on Energy Conversion 2005;20(4):906–15.
[10] Cheng Ying, Qian Chang, Mariesa Crow L, Pekarek Steve, Atcitty Stan. A comparison of diode-clamped and cascaded multilevel converters for a STATCOM with energy storage. IEEE Transactions on Industrial Electronics 2006;53(5):1512–21.
[11] Kai Ding, Yun-ping Zou, Zhan Wang, Zhi-chao Wu, Yun Zhang. A New diode-clamp cascade multilevel converter, the 29th Annual conference of the IEEE Industrial Electronic Society, 2003, pp 2566–2569.
[12] Tremblay Olivier, Louis-Dessaint A, Dekkiche Abdel-Illah. A generic battery model for the dynamic simulation of hybrid electric vehicles. IEEE Vehicle Power and Propulsion conference; 2007:284–9. 14 Seul- Kikim, Jin Hang Jeon, Chang HeeCho, Eung Sang kim, Jong Bo, Modeling and Simulation of Grid connected PV generation system for Electromagnetic Transient Analysis, Solar Energy 83 2009.
[13] Rodríguez José, Lai Jih-Sheng, Peng Fang Zheng. Multilevel inverters: a survey of topologies, controls, and applications. IEEE Transaction of Industrial Electronics 2002;49(4):724–38.
[14] Faete Filho, Yue Cao, Leon M. Tolbert, 11-level cascaded H-bridge grid-tied inverter interface with solar panels, 25Th annual IEEE applied power electronic conference and exposition, 2004, pp 968–972.
[15] Samir Kouro and Bin Wu, Álvaro Moya, Elena Villanueva, Pablo Correa and José, et al, Control of a cascaded H-bridge multilevel converter, for grid connection of photovoltaic systems, 35th annual conference of IEEE industrial electronics, 2009, pp 3976–3982.
[16] Blaabjerg Frede, Jaeger Ulrik, Mu&-Nielsen Stig, Pedersen John K. Power loss in PWM-VSI inverter using NPT or PT IGBT devices. IEEE Transactions on Power Electronics 1995;10(3):358–67.
[17] Data sheet of IGBT module FGH40N60SFD, 600 V, and 40 A. Accessed online, 23-Dec-2010, http://www.fairchildsemi.com/ds/FG%252FFGH40N60SFD.pdf.
[18] IEEE Std C57.110-1998(R2004), IEEE recommended practice for establishing transformer capability when supplying nonsinusoidal load currents.
[19] NEMA ST20-1992 NEMA Premium® efficiency transformer program guidelines program description and specification document. Accessed online, 23-Dec-2010, http://www.nema.org/prod/pwr/trans/transformersProgram.cfm.
[20] Liu Ruifang, Chunting Mi Chris, Wenzhong Gao David. Modeling of iron losses of electrical machines and transformers fed by PWM inverters. IEEE Power Engineering Society General Meeting; 2007. pp 1–7.